

Two-Dimensional Terahertz Spectroscopy of Nonlinear Phononics in the Topological Insulator MnBi_2Te_4

T. G. H. Blank^{1,*}, K. A. Grishunin¹, K. A. Zvezdin^{2,3}, N. T. Hai⁴, J. C. Wu⁴, S.-H. Su⁵, J.-C. A. Huang⁵,
A. K. Zvezdin^{2,6} and A. V. Kimel¹

¹*Institute for Molecules and Materials, Radboud University, 6525 AJ Nijmegen, Netherlands*

²*Prokhorov General Physics Institute of the Russian Academy of Sciences, 119991 Moscow, Russia*

³*HSE University, 101000 Moscow, Russia*

⁴*Department of Physics, National Changhua University of Education, Changhua 500, Taiwan*

⁵*Department of Physics, National Cheng Kung University, Tainan 701, Taiwan*

⁶*New Spintonic Technologies LLC, 121205 Moscow, Russia*

 (Received 1 January 2023; revised 8 March 2023; accepted 5 June 2023; published 14 July 2023)

The interaction of a single-cycle terahertz electric field with the topological insulator MnBi_2Te_4 triggers strongly anharmonic lattice dynamics, promoting fully coherent energy transfer between the otherwise noninteracting Raman-active E_g and infrared (IR)-active E_u phononic modes. Two-dimensional terahertz spectroscopy combined with modeling based on the classical equations of motion and symmetry analysis reveals the multistage process underlying the excitation of the Raman-active E_g phonon. In this nonlinear combined photophononic process, the terahertz electric field first prepares a coherent IR-active E_u phononic state and subsequently interacts with this state to efficiently excite the E_g phonon.

DOI: [10.1103/PhysRevLett.131.026902](https://doi.org/10.1103/PhysRevLett.131.026902)

Although the lattice dynamics of real crystals are rather complex and imply multiple mutual correlations between movements of individual atoms, the modern theory of condensed matter has successfully managed to describe the dynamics in terms of linear superpositions of mutually independent phononic modes. However, if the amplitude of the lattice vibrations is large, this approximation fails and the lattice dynamics enter a poorly explored regime of nonlinear phononics [1–3]. In this regime, a single phonon can be excited by multiple photons and electromagnetic excitation opens up new channels of energy transfer between otherwise noninteracting phononic modes [4–8]. Thanks to recent developments of intense single-cycle terahertz pulses [9–11], the electric field of the latter can exceed 1 MV/cm and has thus become comparable with interatomic fields (~ 100 MV/cm) [12,13]. While such exceptionally intense pulses must facilitate strongly nonlinear interaction of the terahertz electromagnetic fields with the lattice [14–16], there are very few experimental reports on the nonlinear excitation of phonons in this spectral range [1,17–21].

It appears that the family of topological insulators originating from the parent compound Bi_2Te_3 (or Bi_2Se_3) forms an excellent playground to explore nonlinear phononics experimentally [22]. The topological antiferromagnet MnBi_2Te_4 [23] is, in this respect, an especially interesting compound in the family, given the evidence of strong magnetophononic coupling [24,25] and theoretically predicted possibilities to control their topological and magnetic properties using the principles of nonlinear

phononics [26]. Because of the heavy bismuth and tellurium ions, these materials feature several phononic modes in the terahertz spectral range [24,25,27–36], which could enable nonlinear terahertz light-lattice interactions. For instance, it was previously demonstrated that Raman-active phonons in Bi_2Se_3 , which cannot be excited by the electric field of light directly, may still be driven by terahertz electric field via a nonlinear mechanism [22]. In particular, it was suggested that the nonlinear excitation occurred because another IR-active phonon with approximately half the frequency was resonantly driven to so high amplitudes that it could couple nonlinearly to the Raman-active phonon. However, next to this purely phononic mechanism of nonlinearity, state-of-the-art theories also proposed a purely “photonic” [37] and even a combined “photophononic” mechanism [16]. In the former, the Raman-active phonon is excited via the purely photonic nonlinearity known as two-photon absorption. In the combined photophononic mechanism, the photon first excites the IR-active mode, and a second photon interacts with this mode to stimulate energy transfer from the IR-active to the Raman-active mode. The determination of the dominant mechanism in the nonlinear excitation of phonons has so far been a challenge. In this Letter, we resolve this problem by employing two-dimensional (2D) terahertz spectroscopy to reveal the energy flows and thereby the mechanisms behind the nonlinear terahertz light-lattice interactions in MnBi_2Te_4 . The analysis of the 2D spectra and comparison of the outcome with simulations allows us to conclude that the nonlinear excitation of a Raman-active phonon in

MnBi_2Te_4 actually proceeds predominantly via the combined photophononic route.

We studied a 10 nm film of (0001)-oriented MnBi_2Te_4 grown by molecular beam epitaxy on a c -plane $\sim 300 \mu\text{m}$ thick Al_2O_3 substrate (see Ref. [36] for all the details of the growth procedure and characterization of the sample). The sample was capped by 4 nm of MgO to prevent it from oxidizing. The material consists of van der Waals (vdW) coupled septuple layers (SLs) of MnBi_2Te_4 stacked along the out-of-plane direction (z axis). We excited the sample with intense single-cycle terahertz pulses that were generated by tilted pulse-front optical rectification in a LiNbO_3 crystal [9,11], using near-infrared (NIR) pulses with a central wavelength of 800 nm, 4 mJ pulse energy, 1 kHz repetition rate, and 100 fs pulse duration. Using off-axis parabolic mirrors, the generated terahertz pulses were guided and tightly focused onto the sample. The sample was mounted on a cold-finger cryostat, which can be cooled using liquid helium. The terahertz pulses were incident perpendicular to the sample plane, along the vdW stacking z axis, such that the terahertz electric field has only in-plane components. The peak terahertz electric field of 780 kV/cm was calibrated using electro-optical sampling in a $50 \mu\text{m}$ (110)-oriented GaP crystal [38] (see Supplemental Material, Sec. S1 [39]). A weak linearly polarized NIR probe pulse traveled collinearly to the terahertz pump and was focused within the terahertz spot on the sample. The initial probe polarization was set orthogonally to the terahertz electric field. Using a balanced detection scheme and a data-acquisition card [45], we tracked the terahertz pump-induced rotation of the probe polarization $\theta(t)$ as a function of the time delay t between the terahertz pump and probe pulse.

A typical polarization rotation transient induced by a single terahertz pulse at a temperature of 12 K is shown in Fig. 1(a). Two apparent features stand out: an oscillation at a frequency of 3.14 THz (104.7 cm^{-1}) and a terahertz-induced offset with respect to the unperturbed state. Also, we observed a second spike in the signal after $t \approx 9$ ps, which we attributed to the round-trip reflection of the initial terahertz pulse in the substrate. The frequency of the observed mode corresponds to that of a double degenerate Raman-active E_g mode, previously measured in MnBi_2Te_4 [24,31,33–36] or its parent compound Bi_2Te_3 [29] by Raman spectroscopy. It corresponds to in-plane vibrations of the bismuth and tellurium ions as depicted schematically in Fig. 1(b) [25]. We excited and detected highly similar waveforms in a broad range of temperatures from 12 K to room temperature [see Fig. 1(c)]. The observed temperature dependence of the oscillation frequency (see Supplemental Material, Fig. S2 [39]) is in agreement with what is expected for the E_g phonon [29].

Note that the spectrum of the terahertz pulse is sufficiently broad to potentially excite the infrared-active (IR-active) E_u phonon at a frequency of ~ 1.5 THz [32,35].

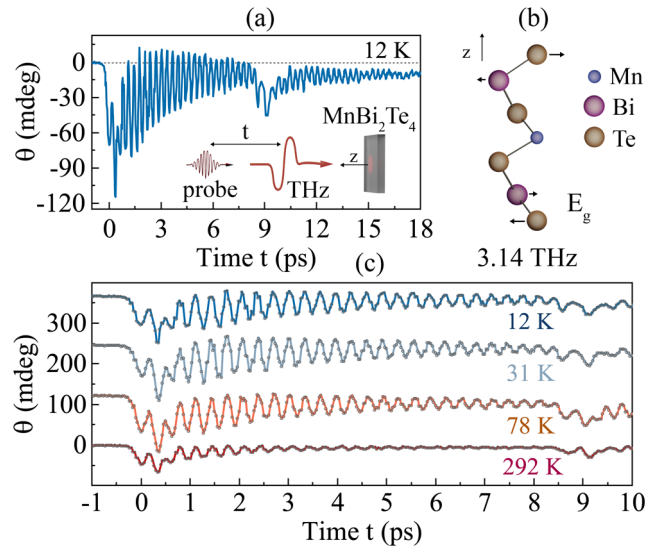


FIG. 1. (a) Dynamics induced by a single terahertz pulse that is measured by changes in the polarization rotation of the probe, performed at a temperature of $T = 12$ K. We attributed the second dip at $t \approx 9$ ps to a terahertz reflection in the substrate. The frequency of the mode corresponds to that of an E_g Raman-active phonon. (b) Single SL of the vdW stacked MnBi_2Te_4 material, showing the displacements of the ions for the Raman-active E_g phonon mode [25]. (c) Waveforms recorded at various temperatures ranging from 12 K to room temperature, showing marginal differences.

However, only Raman-active modes of the E_g species are able to induce birefringence in the medium, which can be explained through the mechanism of so-called “depolarized scattering” [18,46] (see Supplemental Material, Sec. S3 [39]). The resulting time-dependent birefringence induces ellipticity of the probe light, which is subsequently converted to a detectable rotation as a result of static linear birefringence in the sample and substrate. Therefore, although IR-active E_u modes could be excited directly by our terahertz pulses, the experimental setup is only sensitive to Raman-active E_g phonons.

It is remarkable that the frequency of the observed E_g Raman-active phonon lies completely beyond the spectrum of the exciting terahertz pulse [see Fig. 2(a)], which implies that the excitation mechanism is nonlinear. The nonlinearity of the excitation can be further confirmed by measuring the peak Fourier amplitude of the mode at several powers of the terahertz electric field E_{THz} and then fitting this dependence using $|E_{\text{THz}}|^\gamma$ for variable γ . The results are shown in Fig. 2(b) for the temperatures of 12 and 78 K. This shows that the amplitude of the phonon mode scales quadratically $\gamma = 2$ with the applied terahertz field.

Theoretically, as the E_g phonon is Raman active and MnBi_2Te_4 has a centrosymmetric crystal structure, the excitation of the phonon by a terahertz electric field is by symmetry only allowed via a nonlinear mechanism. Note that Raman phonons may become IR active at the interface

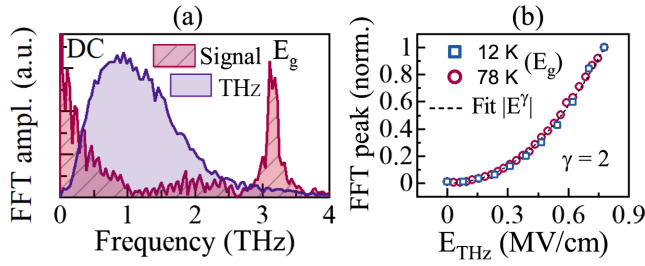


FIG. 2. (a) Fourier amplitudes of the signal [Fig. 1(a)] measured at $T = 12$ K (red), plotted together with the excitation spectrum of the single-cycle terahertz pulse (purple). (b) Normalized peak Fourier amplitude of E_g mode as a function of the applied terahertz electric field, measured at $T = 12$ and 78 K. The fitting emphasizes that the amplitude of the E_g mode scales quadratically with the exciting terahertz field amplitude.

where the inversion symmetry is broken, but this does not hold for purely in-plane vibrations as in the case of the E_g phonon. The interaction between phonons and light is usually described by an interaction potential U , expressed in terms of the electric field of light and of the normal coordinates Q_R for Raman-active phonons and Q_{IR} for IR-active phonons. In linear approximation, we may only include ordinary electric dipole interaction (or electric linear polarizability) of the IR-active phonons, while the interaction energy of the electric field with the Raman-active phonons is strictly equal to zero.

To account for the excitation of a coherent Raman-active phonon, we need to include terms beyond the linear approximation [16]. In the simplest case, the nonlinearity in the thermodynamic potential can be represented by a term that accounts for the high amplitudes of the terahertz pump electric field E . For a fixed terahertz pump polarization, this term is proportional to $Q_R E^2$ and results in a nonlinear optical driving force $dU/dQ_R \propto E^2$ of the Raman-active mode [37]. In the case of ultrashort terahertz pulses, this force will act as a “photonic impact.” Other types of nonlinearity originate from the anharmonic response of the lattice to a terahertz electric field [1,15,16,40]. Suppose that the ultrashort terahertz pulse resonantly excites an IR-active mode Q_{IR} by the electric dipole interaction described by the interaction term $Z^* Q_{\text{IR}} E$, where Z^* is the mode effective charge. When such an IR-active phonon is present, two additional nonlinear terms can be added to the thermodynamic potential which are proportional to $Q_R Q_{\text{IR}} E$ and $Q_R Q_{\text{IR}}^2$. The nonlinear photophononic term $\propto Q_R Q_{\text{IR}} E$ captures how a Raman-active phonon affects the polarizability of the medium through IR-active phonons and enables a nonlinear excitation of the Raman-active mode by terahertz-mediated coupling to the IR-active mode Q_{IR} [16]. In other words, the terahertz electric field first resonantly drives an IR-active mode and subsequently interacts with this mode to promote energy transfer from the IR-active to the Raman-active mode. The nonlinear phononic interaction

term, proportional to $Q_R Q_{\text{IR}}^2$, results from the natural anharmonicity of the interatomic potential and couples Raman-active phonons to IR-active phonons without the need for an external electric field [1,15,40]. The driving force of the Raman-active mode in this case is proportional to the square of the amplitude of the IR-active mode $dU/dQ_R \propto Q_{\text{IR}}^2$. Altogether, when considering one IR-active and one Raman-active mode in a centrosymmetric medium, the interaction potential beyond linear approximation would thus acquire the following form:

$$U = -Z^* Q_{\text{IR}} E - b Q_R Q_{\text{IR}} E - c Q_R Q_{\text{IR}}^2 - \delta_R Q_R E^2, \quad (1)$$

where b , c , and δ_R are phenomenological constants. For the normal coordinates of the Raman- and IR-active phonons ($\nu = R, \text{IR}$), the corresponding equations of motion are of the form

$$\ddot{Q}_\nu + \Gamma_\nu \dot{Q}_\nu + \omega_\nu^2 Q_\nu = -\frac{dU}{dQ_\nu}, \quad (2)$$

where $\Gamma_\nu = 2\zeta_\nu \omega_\nu$ are the damping coefficients and ζ_ν are the dimensionless damping ratios.

In order to reveal the origin of the experimentally observed nonlinear excitation of the E_g phonon, we performed 2D terahertz spectroscopy [18,47,48]. In this pump-probe technique, we employ two terahertz pump pulses instead of one, mutually separated in time by the “excitation time” τ . The polarization rotation $\theta_{12}(t, \tau)$ of a NIR probe pulse induced by the two terahertz pulses was mapped as a function of both probe delay t and the excitation time τ . The two-dimensional mapping of this measurement is shown in Fig. 3(a). It clearly shows the oscillations, which we assigned to the E_g mode, as well as the signals associated with the reflected terahertz pulses. At the same time, our experimental setup tracked the signals from pump 1 [$\theta_1(t, \tau)$] and pump 2 [$\theta_2(t, \tau)$] separately. Combining the three signals allowed us to calculate the—by definition—nonlinear contribution to the signal [48–51],

$$\theta_{\text{NL}}(t, \tau) = \theta_{12}(t, \tau) - \theta_1(t, \tau) - \theta_2(t, \tau). \quad (3)$$

The result of this measurement is shown in Fig. 3(b), emphasizing the large degree of nonlinearity of the E_g mode.

The method reveals how the amplitude of the excited Raman-active E_g phonon changes as a function of τ . These changes become clearly visible when taking the two-dimensional fast Fourier transform (2D FFT) of $\theta_{\text{NL}}(t, \tau)$ to obtain the normalized 2D Fourier amplitude $\tilde{\theta}_{\text{NL}}(f_{\text{det}}, f_{\text{ex}})$, where the detection frequency f_{det} and the excitation frequency f_{ex} are the conjugate variables of t and τ , respectively. When the E_g mode with frequency ω_R is driven momentarily after the terahertz pulse arrival by two oscillators $\Omega_{1,2}$ at frequencies $\omega_{1,2}$, with a force term of the

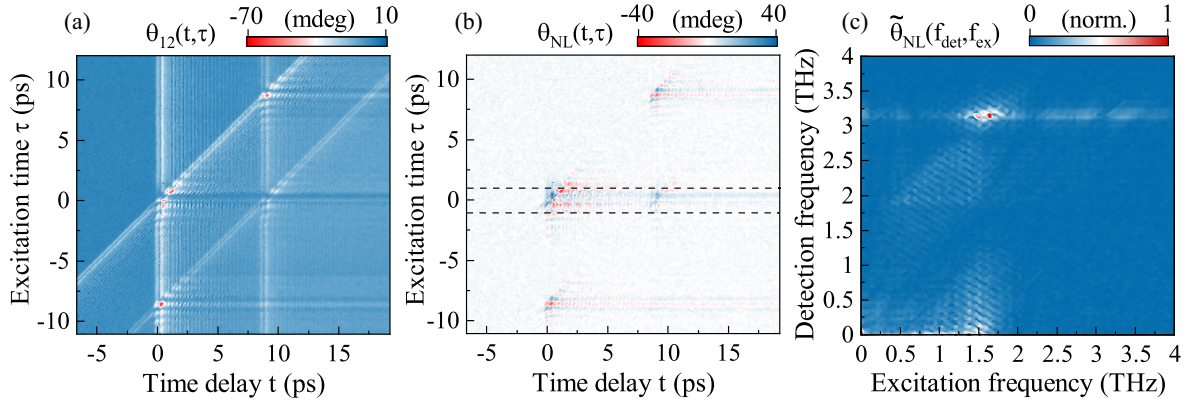


FIG. 3. (a) 2D mapping of the polarization rotation $\theta_{12}(t, \tau)$ as a function of t and pump-pump delay τ . Besides the initial overlap and the modulations due to the E_g mode, one can clearly see the internally reflected pulses as we observed in Fig. 1. (b) The extracted nonlinear contribution $\theta_{NL}(t, \tau)$ to the signal. The largest degree of nonlinearity is observed when the pulses (reflected or initial) overlap. In further analysis, we excluded the region between $\tau = \pm 1$ (indicated by the black dashed lines) to avoid artifacts as a result of the simultaneous presence of two pulses in the terahertz generating LiNbO₃ crystal (see Supplemental Material, Sec. S4 [39] for a detailed explanation). (c) 2D FFT of the nonlinear signal $\theta_{NL}(t, \tau)$. The result reveals two peaks at the detection frequency of the E_g phonon (3.14 THz) at the excitation frequencies of approximately 1.47 and 1.67 THz.

form $\propto \Omega_1(\omega_1)\Omega_2(\omega_2)$ that obeys the resonant condition $\omega_1 + \omega_2 = \omega_R$, two clear peaks should appear in the excitation spectrum centered around the frequencies ω_1 and ω_2 (see Supplemental Material, Sec. S5 [39]). The result for $\tilde{\theta}_{NL}(f_{\text{det}}, f_{\text{ex}})$ is shown in Fig. 3(c). Indeed, we observed two peaks at the detection frequency $f_{\text{det}} = 3.14$ THz of the E_g mode, for the excitation frequencies of approximately $f_{\text{ex}} = 1.47$ and 1.67 THz, whose sum equals the frequency of the E_g mode (3.14 THz).

As was discussed above, the nonlinear excitation of the E_g phonon can occur via three different mechanisms—photonic, phononic, and combined photophononic. Therefore, we performed simulations with each of the corresponding driving forces separately, using the two coupled equations of motion from Eq. (2) and using realistic shapes of the terahertz electric field pulses while including the substrate reflections (see Supplemental Material, Sec. S6 [39] for all the details). The comparison of the 2D FFT of the experimental data with that of the simulations is shown in Fig. 4(a). First, the narrow bandwidth in the experimental excitation spectrum allows us to exclude the purely photonic mechanism with driving force $\propto E^2$. The 2D spectrum of such a nonlinear mechanism reflects the broadband spectrum of the pump electric field [see Fig. 2(a)]. That is, for every frequency ω_1 in the entire single-cycle terahertz spectrum, another frequency ω_2 can be found such that they fulfill the resonance condition $\omega_1 + \omega_2 = \omega_R$, and the resulting excitation spectrum will thus be very broad. This is confirmed by the simulation result of photonic impact $\propto E^2$ seen in Fig. 4(a). Opposed to this, the excitation spectra of the combined photophononic driving force $\propto Q_{\text{IR}}E$ and purely phononic mechanism $\propto Q_{\text{IR}}^2$ can be very narrow due to the

typically long lifetime and thus narrow spectral lines of phonons. Therefore, we included an IR-active phonon with normal coordinate Q_{IR} and frequency $f_{E_u} = 1.47$ THz, which we assigned to an E_u IR-active phonon mode in accordance with earlier studies based on density functional theory [35] and IR spectroscopy [32]. It can be seen in Fig. 4(a) that the photophononic driving term $\propto Q_{\text{IR}}E$ produces two peaks that are highly similar to the experimental result. The purely phononic driving term $\propto Q_{\text{IR}}^2$ also produces these two peaks but has an additional spectral component away from the detection frequency of 3.14 THz [see Fig. 4(a)], something that is not seen in the experiment. By reducing the IR-active phonon damping, this latter spectral component becomes even more apparent, and the purely phononic mechanism becomes significantly different and clearly distinguishable from the photophononic mechanism (see Supplemental Material, Sec. S6 [39]). However, when instead increasing the IR-active phonon damping, the results of Q_{IR}^2 and $Q_{\text{IR}}E$ become effectively identical and both depict the clear two-peak structure. This can be understood by the fact that, during the presence of the terahertz pulse, the IR-active phonon undergoes a forced oscillation $Q_{\text{IR}}(t) \propto E(t)$, such that the off-resonant term Q_{IR}^2 effectively reduces to $Q_{\text{IR}}E$ to fulfill the resonance condition. If the damping of the phonon is large, the “free” driving force $\propto Q_{\text{IR}}^2$ after the pulse excitation decays fast, meaning that the spectra of the two driving forces proportional to $Q_{\text{IR}}E$ and Q_{IR}^2 are very similar. Therefore, it can be concluded that a sufficient agreement between simulations and experiment can be obtained when accounting only for the driving term $\propto Q_{\text{IR}}E$ and that the photophononic pathway of excitation is dominant. Two-dimensional spectroscopy thereby

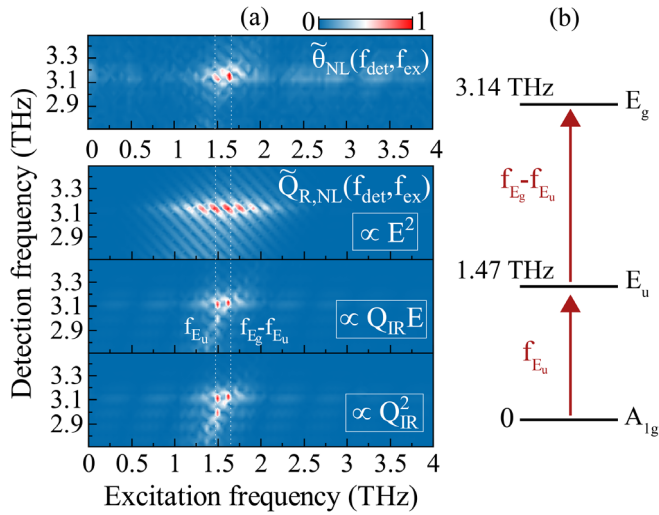


FIG. 4. (a) Upper: normalized 2D FFT of the experimental signal $\theta_{NL}(t, \tau)$. Lower: normalized 2D FFT of the nonlinear part of the simulated $Q_{R,NL}(t, \tau)$ modeled by the equations of motion (2), taking the linear interaction term $\propto Z^* Q_{IR} E$ and the three separate nonlinear photonic $\propto E^2$, photophononic $\propto Q_{IR} E$, and phononic $\propto Q_{IR}^2$ driving forces into account. The best agreement of the simulations with the experimental data is obtained with the driving term $\propto Q_{IR} E$, which confirms that the excitation of the Raman-active E_g phonon is mediated by the IR-active E_u phonon via the photophononic mechanism. For future studies, we note that the substrate-reflected terahertz pulses may influence the results drastically. In particular, the presence of reflections precludes directly reading off frequencies from the 2D FFT spectra. This can be seen in the Supplemental Material [39], where we show simulation results for different traveling times of the reflected pulses as well as simulation results without reflections. (b) Schematic illustration of the excitation mechanism in a model with two oscillators, corresponding to the E_u phonon and E_g phonon. The arrows indicate the stimulated transitions.

revealed the actual flow of energy in the nonlinear phononics of $MnBi_2Te_4$ as shown schematically in Fig. 4(b), in which the terahertz electric field first generates a coherent E_u phonon and afterward interacts with this phonon to excite the E_g Raman-active phonon.

In summary, we showed that a single-cycle terahertz electric field triggers strongly anharmonic lattice dynamics, which initiates a light-mediated interaction between otherwise noninteracting phonons. The discovery of this nonlinear photophononic mechanism in the topological antiferromagnet $MnBi_2Te_4$ in the terahertz spectral range, where the lattice is tightly connected to topological and magnetic properties [26], opens up a plethora of opportunities for the field of nonlinear phononics and the lattice engineering of topological matter [3], enabling new routes for the ultrafast manipulation of complex quantum phases.

The authors acknowledge E. A. Mashkovich for his contribution to the development of the 2D terahertz

spectroscopy experimental setup. The authors thank Sergey Semin and Chris Berkhout for technical support and Mike Gould for editorial assistance. The work was supported by the Dutch Research Council (NWO), the Gravitation program of the Dutch Ministry of Education, Culture and Science (OCW) under the research program ‘‘Materials for the Quantum Age’’ (QuMat) Registration No. 024.005.006, the European Research Council ERC Grant Agreement No. 101054664 273 (SPARTACUS), and the Russian Science Foundation Grant No. 22-12-00367. The authors declare that this work has been published as a result of peer-to-peer scientific collaboration between researchers. The provided affiliations represent the actual addresses of the authors in agreement with their digital identifier (ORCID) and cannot be considered as a formal collaboration between the aforementioned institutions.

*Corresponding author.

thomas.blank@ru.nl

- [1] M. Först, C. Manzoni, S. Kaiser, Y. Tomioka, Y. Tokura, R. Merlin, and A. Cavalleri, Nonlinear phononics as an ultrafast route to lattice control, *Nat. Phys.* **7**, 854 (2011).
- [2] D. Nicoletti and A. Cavalleri, Nonlinear light–matter interaction at terahertz frequencies, *Adv. Opt. Photonics* **8**, 401 (2016).
- [3] A. S. Disa, T. F. Nova, and A. Cavalleri, Engineering crystal structures with light, *Nat. Phys.* **17**, 1087 (2021).
- [4] A. A. Maradudin and R. F. Wallis, Ionic Raman effect. I. Scattering by localized vibration modes, *Phys. Rev. B* **2**, 4294 (1970).
- [5] R. F. Wallis and A. A. Maradudin, Ionic Raman effect. II. The first-order ionic Raman effect, *Phys. Rev. B* **3**, 2063 (1971).
- [6] T. P. Martin and L. Genzel, Ionic Raman scattering and ionic frequency mixing, *Phys. Status Solidi (b)* **61**, 493 (1974).
- [7] D. L. Mills, Ionic contributions to the Raman tensor of insulators, *Phys. Rev. B* **35**, 9278 (1987).
- [8] M. Först, R. Mankowsky, and A. Cavalleri, Mode-selective control of the crystal lattice, *Acc. Chem. Res.* **48**, 380 (2015).
- [9] J. Hebling, G. Almási, I. Z. Kozma, and J. Kuhl, Velocity matching by pulse front tilting for large-area THz-pulse generation, *Opt. Express* **10**, 1161 (2002).
- [10] M. C. Hoffmann and J. A. Fülöp, Intense ultrashort terahertz pulses: Generation and applications, *J. Phys. D* **44**, 083001 (2011).
- [11] H. Hirori, A. Doi, F. Blanchard, and K. Tanaka, Single-cycle terahertz pulses with amplitudes exceeding 1 MV/cm generated by optical rectification in $LiNbO_3$, *Appl. Phys. Lett.* **98**, 091106 (2011).
- [12] C. Kittel, P. McEuen, and P. McEuen, *Introduction to Solid State Physics* (Wiley, New York, 1996), Vol. 8, Chap. 3.
- [13] B. Qiu and X. Ruan, Molecular dynamics simulations of lattice thermal conductivity of bismuth telluride using two-body interatomic potentials, *Phys. Rev. B* **80**, 165203 (2009).

- [14] P. Salén, M. Basini, S. Bonetti, J. Hebling, M. Krasilnikov, A. Y. Nikitin, G. Shamuilov, Z. Tibai, V. Zhaunerchyk, and V. Goryashko, Matter manipulation with extreme terahertz light: Progress in the enabling THz technology, *Phys. Rep.* **836–837**, 1 (2019).
- [15] A. Subedi, A. Cavalleri, and A. Georges, Theory of nonlinear phononics for coherent light control of solids, *Phys. Rev. B* **89**, 220301(R) (2014).
- [16] G. Khalsa, N. A. Benedek, and J. Moses, Ultrafast Control of Material Optical Properties via the Infrared Resonant Raman Effect, *Phys. Rev. X* **11**, 021067 (2021).
- [17] D. M. Juraschek and S. F. Maehrlein, Sum-frequency ionic Raman scattering, *Phys. Rev. B* **97**, 174302 (2018).
- [18] C. L. Johnson, B. E. Knighton, and J. A. Johnson, Distinguishing Nonlinear Terahertz Excitation Pathways with Two-Dimensional Spectroscopy, *Phys. Rev. Lett.* **122**, 073901 (2019).
- [19] M. Kozina, M. Fechner, P. Marsik, T. van Driel, J. M. Glowia, C. Bernhard, M. Radovic, D. Zhu, S. Bonetti, U. Staub, and M. C. Hoffmann, Terahertz-driven phonon up-conversion in SrTiO₃, *Nat. Phys.* **15**, 387 (2019).
- [20] A. S. Disa, M. Fechner, T. F. Nova, B. Liu, M. Först, D. Prabhakaran, P. G. Radaelli, and A. Cavalleri, Polarizing an antiferromagnet by optical engineering of the crystal field, *Nat. Phys.* **16**, 937 (2020).
- [21] H.-W. Lin, G. Mead, and G. A. Blake, Mapping LiNbO₃ Phonon-Polariton Nonlinearities with 2D THz-THz-Raman Spectroscopy, *Phys. Rev. Lett.* **129**, 207401 (2022).
- [22] A. A. Melnikov, K. N. Boldyrev, Y. G. Selivanov, V. P. Martovitskii, S. V. Chekalin, and E. A. Ryabov, Coherent phonons in a Bi₂Se₃ film generated by an intense single-cycle THz pulse, *Phys. Rev. B* **97**, 214304 (2018).
- [23] M. Otrokov, I. Klimovskikh, H. Bentmann *et al.*, Prediction and observation of an antiferromagnetic topological insulator, *Nature (London)* **576**, 416 (2019).
- [24] J. Choe, D. Lujan, M. Rodriguez-Vega, Z. Ye, A. Leonardo, J. Quan, T. N. Nunley, L.-J. Chang, S.-F. Lee, J. Yan, G. A. Fiete, R. He, and X. Li, Electron-phonon and spin-lattice coupling in atomically thin layers of MnBi₂Te₄, *Nano Lett.* **21**, 6139 (2021).
- [25] H. Padmanabhan, M. Poore, P. K. Kim, N. Z. Koocher, V. A. Stoica, D. Puggioni, H. (Hugo) Wang, X. Shen, A. H. Reid, M. Gu, M. Wetherington, S. H. Lee, R. D. Schaller, Z. Mao, A. M. Lindenberg, X. Wang, J. M. Rondinelli, R. D. Averitt, and V. Gopalan, Interlayer magnetophononic coupling in MnBi₂Te₄, *Nat. Commun.* **13**, 1929 (2022).
- [26] M. Rodriguez-Vega, Z.-X. Lin, A. Leonardo, A. Ernst, M. G. Vergniory, and G. A. Fiete, Light-driven topological and magnetic phase transitions in thin layer antiferromagnets, *J. Phys. Chem. Lett.* **13**, 4152 (2022).
- [27] J. O. Jenkins, J. A. Rayne, and R. W. Ure, Elastic moduli and phonon properties of Bi₂Te₃, *Phys. Rev. B* **5**, 3171 (1972).
- [28] H. Rauh, R. Geick, H. Kohler, N. Nucker, and N. Lehner, Generalized phonon density of states of the layer compounds Bi₂Se₃, Bi₂Te₃, Sb₂Te₃ and Bi₂(Se_{0.5}Te_{0.5})₃, (Bi_{0.5}Sb_{0.5})₂Te₃, *J. Phys. C* **14**, 2705 (1981).
- [29] P. Mal, G. Bera, G. R. Turpu, S. K. Srivastava, A. Gangan, B. Chakraborty, B. Das, and P. Das, Vibrational spectra of Pb₂Bi₂Te₃, PbBi₂Te₄, and PbBi₄Te₇ topological insulators: temperature-dependent Raman and theoretical insights from DFT simulations, *Phys. Chem. Chem. Phys.* **21**, 15030 (2019).
- [30] A. dos Santos Silva, É. V. Guimarães, N. F. Cano, and R. S. da Silva, Study of vibrational properties of Bi_{2-x}Mn_xTe₃ nanocrystals in host glass: Effect of xMn-concentration, *J. Raman Spectrosc.* **53**, 95 (2022).
- [31] C. Pei, Y. Xia, J. Wu, Y. Zhao, L. Gao, T. Ying, B. Gao, N. Li, W. Yang, D. Zhang, H. Gou, Y. Chen, H. Hosono, G. Li, and Y. Qi, Pressure-induced topological and structural phase transitions in an antiferromagnetic topological insulator, *Chin. Phys. Lett.* **37**, 066401 (2020).
- [32] B. Xu, Y. Zhang, E. H. Alizade, Z. A. Jahangirli, F. Lyzwa, E. Sheveleva, P. Marsik, Y. K. Li, Y. G. Yao, Z. W. Wang, B. Shen, Y. M. Dai, V. Kataev, M. M. Otrokov, E. V. Chulkov, N. T. Mamedov, and C. Bernhard, Infrared study of the multiband low-energy excitations of the topological antiferromagnet MnBi₂Te₄, *Phys. Rev. B* **103**, L121103 (2021).
- [33] Y. Cho, J. H. Kang, L. Liang, M. Taylor, X. Kong, S. Ghosh, F. Kargar, C. Hu, A. A. Balandin, A. A. Puretzky, N. Ni, and C. W. Wong, Phonon modes and Raman signatures of MnBi_{2n}Te_{3n+1} ($n = 1, 2, 3, 4$) magnetic topological heterostructures, *Phys. Rev. Res.* **4**, 013108 (2022).
- [34] Z. S. Aliev, I. R. Amiraslanov, D. I. Nasonova, A. V. Shevelkov, N. A. Abdullayev, Z. A. Jahangirli, E. N. Orujlu, M. M. Otrokov, N. T. Mamedov, M. B. Babanly, and E. V. Chulkov, Novel ternary layered manganese bismuth tellurides of the MnTe – Bi₂Te₃ system: Synthesis and crystal structure, *J. Alloys Compd.* **789**, 443 (2019).
- [35] A. Kobiałka, M. Sternik, and A. Ptok, Dynamical properties of the magnetic topological insulator TBi₂Te₄ ($T = \text{Mn, Fe}$): Phonons dispersion, Raman active modes, and chiral phonons study, *Phys. Rev. B* **105**, 214304 (2022).
- [36] S.-H. Su, J.-T. Chang, P.-Y. Chuang, M.-C. Tsai, Y.-W. Peng, M. K. Lee, C.-M. Cheng, and J.-C. A. Huang, Epitaxial growth and structural characterizations of MnBi₂Te₄ thin films in nanoscale, *Nanomater. Nanotechnol.* **11**, 3322 (2021).
- [37] S. Maehrlein, A. Paarmann, M. Wolf, and T. Kampfrath, Terahertz Sum-Frequency Excitation of a Raman-Active Phonon, *Phys. Rev. Lett.* **119**, 127402 (2017).
- [38] A. Leitenstorfer, S. Hunsche, J. Shah, M. C. Nuss, and W. H. Knox, Detectors and sources for ultrabroadband electro-optic sampling: Experiment and theory, *Appl. Phys. Lett.* **74**, 1516 (1999).
- [39] See Supplemental Material at <http://link.aps.org/supplemental/10.1103/PhysRevLett.131.026902> for details on the calibration of terahertz pulses in GaP, for the single terahertz pump-induced waveforms as a function of temperature, pump and probe polarization, and terahertz amplitude, for details of the point-group D_{3d} , and for a detailed treatment of analytical and numerical modeling of the nonlinear excitation of the Raman-active phonon, which includes Refs. [16,18,29,30,35,38,40–44].
- [40] D. M. Juraschek, M. Fechner, and N. A. Spaldin, Ultrafast Structure Switching through Nonlinear Phononics, *Phys. Rev. Lett.* **118**, 054101 (2017).
- [41] S. Casalbuoni, H. Schlarb, B. Schmidt, B. Steffen, P. Schmuser, and A. Winter, Numerical studies on the

- electro-optic sampling of relativistic electron bunches, in *Proceedings of the 2005 Particle Accelerator Conference* (2005), pp. 3070–3072.
- [42] S. L. Altmann and P. Herzig, *Point-Group Theory Tables* (Oxford University Press, New York, 1994).
- [43] M. Rodriguez-Vega, A. Leonardo, and G. A. Fiete, Group theory study of the vibrational modes and magnetic order in the topological antiferromagnet MnBi_2Te_4 , *Phys. Rev. B* **102**, 104102 (2020).
- [44] R. Loudon, The Raman effect in crystals, *Adv. Phys.* **13**, 423 (1964).
- [45] C. A. Werley, S. M. Teo, and K. A. Nelson, Pulsed laser noise analysis and pump-probe signal detection with a data acquisition card, *Rev. Sci. Instrum.* **82**, 123108 (2011).
- [46] S. P. S. Porto, J. A. Giordmaine, and T. C. Damen, Depolarization of Raman scattering in calcite, *Phys. Rev.* **147**, 608 (1966).
- [47] M. Woerner, W. Kuehn, P. Bowlan, K. Reimann, and T. Elsaesser, Ultrafast two-dimensional terahertz spectroscopy of elementary excitations in solids, *New J. Phys.* **15**, 025039 (2013).
- [48] J. Lu, X. Li, Y. Zhang, H. Y. Hwang, B. K. Ofori-Okai, and K. A. Nelson, Two-dimensional spectroscopy at terahertz frequencies, *Top. Curr. Chem.* **376**, 6 (2018).
- [49] K. Reimann, M. Woerner, and T. Elsaesser, Two-dimensional terahertz spectroscopy of condensed-phase molecular systems, *J. Chem. Phys.* **154**, 120901 (2021).
- [50] M. Woerner, A. Ghalgaoui, K. Reimann, and T. Elsaesser, Two-color two-dimensional terahertz spectroscopy: A new approach for exploring even-order nonlinearities in the non-perturbative regime, *J. Chem. Phys.* **154**, 154203 (2021).
- [51] E. A. Mashkovich, K. A. Grishunin, R. M. Dubrovin, A. K. Zvezdin, R. V. Pisarev, and A. V. Kimel, Terahertz light-driven coupling of antiferromagnetic spins to lattice, *Science* **374**, 1608 (2021).